Adsorption (2014) 20:359–371
DOI 10.1007/s10450-013-9573-9

# Modeling water vapor adsorption/desorption cycles

**Max Hefti · Marco Mazzotti**

Received: 23 May 2013 / Accepted: 29 August 2013 / Published online: 24 October 2013


**Abstract** This modeling work deals with the adsorption of water vapor on different porous materials where it undergoes capillary condensation and its adsorption/desorption isotherms exhibit hysteresis. The focus is on the description of the so called scanning curves, i.e. the adsorption/desorption isotherms observed when such an adsorbent is repeatedly loaded and unloaded in a range of conditions where hysteresis is observed, and on the simulation of fixed bed adsorption/desorption cycles. We use an approach originally developed by Štěpánek et al. (Chem Eng Sci 55(2):431–440, 2000), and expand it so as to include more general isotherms (not only the Dubinin–Radushkevich and Dubinin–Astakhov model, but also the Guggenheim–Anderson–de Boer model and the Do and Do model) and to allow for less than infinitely fast heat transfer, so as to consider non-isothermal situations. From a modeling point of view the results are satisfactory and highlight the need for better experimental data on water vapor adsorption, which need to be measured in enhanced experimental set-ups, capable to tightly control the relative humidity of the gas phase.

**Keywords** Water adsorption · Hysteresis · Scanning curves · Fixed bed

## 1 Introduction

Water vapor is present in many streams treated in gas adsorption separation processes, e.g. in the flue gas of power plants implementing either post-combustion or pre-combustion carbon dioxide capture schemes. The adsorptivity of water in many commercial adsorbents not only plays a beneficial role but also constitutes a problem that has to be overcome. As compared to adsorption of technical gases, water adsorption is special in at least three ways. Firstly, water can undergo capillary condensation in porous solids and thus may exhibit a hysteresis loop in the adsorption isotherms, i.e. the adsorbent loading and regeneration follow different paths in the adsorbed phase concentration versus partial pressure space. Secondly, by and large the effect of temperature on the adsorbed amount manifests itself through the relative humidity of the gas phase, i.e. adsorption isotherms at any temperature coincide when the adsorbed phase concentration is expressed in terms of relative humidity rather than of water partial pressure. Finally, measuring adsorption of pure water vapor or of any other gas in the presence of water vapor is technically challenging, hence the lack of comprehensive and accurate water adsorption data.

While experimental efforts are underway in many groups including ours, in this work we would like to focus on theoretical and modeling aspects.

When facing the need to model adsorption separation processes, or simply fixed bed adsorption/desorption cycles, in the presence of water one must give a mathematical expression not only to its primary adsorption and primary desorption isotherms, but also to the secondary ones, the so called scanning curves, i.e. the adsorbed phase water concentration evolution undergone during regeneration or loading of a partially saturated or partially regenerated adsorbent, respectively. Moreover, one must incorporate these effects into the mathematical model of the fixed bed, where as a consequence of hysteresis the state of a pore and of an adsorbent particle depends not only on the current composition and temperature of the gas phase, but also on its adsorption/desorption history; in other words the simulation

M. Hefti · M. Mazzotti (✉)
Institute of Process Engineering, ETH Zurich, Sonneggstrasse 3, 8092 Zurich, Switzerland
e-mail: marco.mazzotti@ipe.mavt.ethz.ch

code must keep memory of the past to be able to describe the present state and the future evolution.

There is a line of research that has dealt successfully with these issues, starting from the seminal work by Mason on the description of capillary condensation and the developments of primary and secondary adsorption and desorption isotherms, using the concept of pore size distributions and percolation theory (Mason 1983, 1988). Then Rajniak and Yang (1993, 1994) extended Mason's work to describe not only secondary but also higher order adsorption and desorption scanning curves. Finally, Štěpánek et al. (2000) were able to obtain a simpler and less complex relationship to calculate scanning curves and to plug this into a fixed bed model; thus, they were able to simulate adsorption and desorption in a fixed bed and simple pressure swing adsorption cycles, under isothermal conditions and for one specific isotherm.

We consider the work briefly summarized above as very important and useful. Therefore, we believe that it is important to extend that approach to a larger number of adsorption isotherms and to apply it not only to isothermal conditions, but also to situations where the temperature varies and the material balance considered earlier (Štěpánek et al. 2000) is coupled to the energy balance, i.e. adiabatic columns and thermostatted columns. These are the objectives of this work, where after a summary of the theory, we apply it to three different isotherms. Then we plug these into a column model, consisting of material and energy balances, and we simulate adsorption and desorption cycles under different heat transfer scenarios.

## 2 Background

Based on previous work by Mason (1983, 1988) and Rajniak and Yang (1993, 1994, 1996), Štěpánek et al. (2000) proposed a method to model higher order isotherms—or scanning curves—in hysteresis-dependent isotherms. They used equations introduced in Rajniak and Yang (1994) and applied the method to the dual Dubinin–Radushkevich and Dubinin–Astakhov isotherm model.

A hysteresis dependent isotherm consists of a primary adsorption branch and a primary desorption branch. The hysteresis loop is delimited by the lower and the upper closure point, which define the range of validity of the primary desorption branch. The primary adsorption branch is labelled with the subscript 'A', while the primary desorption branch is labelled with the subscript 'D'. The concentration variable $x$ is the partial pressure or the relative humidity in case of water vapor hence it is defined between zero and one. At the lower closure point the adsorbed amount is $n_L$ at relative humidity $x_L$, while at the upper closure point the adsorbed amount is $n_U$ at relative humidity $x_U$. Given an equation for a primary adsorption isotherm, $n_A(x)$, the corresponding equation for the description of the primary desorption branch is chosen to be of the form, $n_D(x - x_L)$. The definitions of the general primary isotherm equations, their range of validity and the closure points are as follows:

$$
\begin{aligned}
&n_A = n_A(x) \quad 0 \le x \le 1 \\
&n_D = \begin{cases} n_A(x) & x < x_L \text{ or } x > x_U \\ n_D(x - x_L) & x_L \le x \le x_U \end{cases} \\
&\text{with } n_D(0) = n_L = n_A(x_L) \\
&\quad n_D(x_U - x_L) = n_U = n_A(x_U)
\end{aligned}
\tag{1}
$$

Three examples of adsorption isotherms exhibiting hysteresis are illustrated in Fig. 1.

### 2.1 Higher order adsorption isotherms

A second order adsorption scanning curve emerges from the primary desorption branch within the hysteresis loop. Third and higher order adsorption scanning curves emerge from a turning point within the hysteresis loop. Note that a turning point is a state along an adsorption or desorption isotherm when the prevailing mechanism is reversed, i.e. the system (or the particle, or the pore) switches from adsorption to desorption or vice versa.

A general adsorption process starting at the turning point $(x_{2k-1}, n_{2k-1})$ is given by

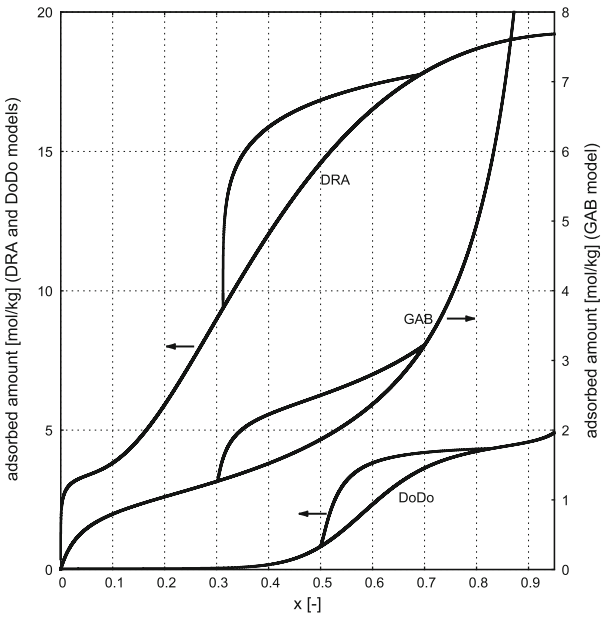


**Fig. 1** Primary adsorption and desorption isotherms of the DRA, GAB and DoDo models. For the sake of clarity, the DRA and DoDo models are plotted against the *left y-axis*, while the GAB model is plotted against the *right y-axis* as indicated by the *arrows*

$$n_a(x) = \frac{n_{2k-1}n_{A,2k-2} - n_{2k-2}n_{A,2k-1}}{n_{A,2k-2} - n_{A,2k-1}} + \frac{n_{2k-2} - n_{2k-1}}{n_{A,2k-2} - n_{A,2k-1}} n_A(x) \quad (2)$$

where the subscript 'a' indicates a higher order adsorption isotherm. This expression was first derived on the basis of the pore-blocking theory by Rajniak and Yang (1994) and is based on previous work by Mason (1983, 1988). Straightforward manipulations lead to another useful form of Eq. (2), i.e.

$$n_a(x) = n_{2k-1} + b\left[n_A(x) - n_{A,2k-1}\right] \quad (3)$$

where the scaling factor $b$ is defined as:

$$b = \frac{n_{2k-2} - n_{2k-1}}{n_{A,2k-2} - n_{A,2k-1}} \quad (4)$$

These expressions make it obvious that the adsorption branch evolves from the point $n_{2k-1}$ and the second term describes the scaling of the difference of the adsorbed amount as predicted by the primary adsorption branch at humidity $x$ and $x_{2k-1}$ by the scaling factor $b$. This equation is general and may be applied to any adsorption isotherm. Note that in the case of a secondary adsorption scanning curve the point $(x_{2k-1}, n_{2k-1})$ belongs to the primary desorption isotherm and $(x_{2k-2}, n_{2k-2})$ is the upper closure point of the hysteresis loop.

## 2.2 Higher order desorption isotherms

A general higher order desorption process, starting at point $(x_{2k}, n_{2k})$ is given by:

$$n_d(x) = n_{2k-1} + n(x - x_{2k-1}) \quad (5)$$

where the subscript 'd' indicates a higher order desorption isotherm. $n_{2k-1}$ is the previous turning point and $n(x - x_{2k-1})$ is conveniently chosen to be of the form of the primary desorption isotherm and depends on different parameters to describe the possible paths within the hysteresis loop. To calculate such parameters in the case of a generic desorption scanning curve, two conditions are enforced at the turning point $(x_{2k}, n_{2k})$. The first condition is based on the similarity hypothesis, that is the desorption scanning curves resemble the primary desorption branch in their geometrical features. Štěpánek et al. (2000) proposed a relationship that gives the slope $\sigma_{2k}$ of a general desorption scanning curve starting at point $(x_{2k}, n_{2k})$ in terms of the slope of the previous desorption branch, $\sigma_{2k-2}$, that started at point $(x_{2k-2}, n_{2k-2})$, as:

$$\sigma_{2k} = b\left.\frac{\partial n_A}{\partial x}\right|_{x_{2k}} - \varphi\left[b\left.\frac{\partial n_A}{\partial x}\right|_{x_{2k-2}} - \sigma_{2k-2}\right] \quad (6)$$

where $\varphi$ is a measure of the fraction of pores that are filled, which is defined as:

$$\varphi = \frac{n_{2k} - n_{2k-1}}{n_{2k-2} - n_{2k-1}} \quad (7)$$

Although not explicitly specified by Štěpánek et al. (2000), the basis of the empirical equation (6) appears to be the similarity hypothesis first proposed by Philip (1964) and later extended by Mualem (1973) and Mualem and Beriozkin (2009). Philip (1964) emphasizes that the similarity hypothesis does not have a strict physical meaning, thus being essentially empirical. The second condition was taken directly from Rajniak and Yang (1994) and exploits the fact that the adsorption and desorption scanning curves must intersect at the turning point $(x_{2k}, n_{2k})$. The parameters are therefore calculated as solution of the two equations:

$$\begin{cases} \left.\frac{dn_d}{dx}\right|_{x_{2k}} = \sigma_{2k} \\ n_d(x_{2k}) = n_a(x_{2k}) \end{cases} \quad (8)$$

Assuming an explicit expression for the desorption isotherm $n_d(x)$ with two variable parameters, this system yields the needed values of the parameters, and possibly analytical relationships for them, as shown in detail through the three examples presented in Sect. 3.

## 2.3 Discussion

Before applying the approach developed by Štěpánek et al. (2000) as described above, it is worth making a few remarks to fully appreciate its merits.

Mason developed relationships that could describe both secondary adsorption and secondary desorption isotherms as a function of the connectivity of the pore network, which is assumed to be constant and has to be determined through experiments. He realized however that while on the one hand the adsorption scanning curves were qualitatively close to the available experimental data, the desorption scanning curves exhibited major qualitative deviations. He then called the latter curves just "theoretical" isotherms, and derived the "real isotherms" by correcting the theoretical ones through a term proportional to $(-\ln(x_U/x))$ (Mason 1988); Rajniak and Yang (1993) followed the same approach. Such term provides qualitatively the observed adequate correction, but suffers from two major problems: there is an additional purely empirical parameter, and the desorption scanning curves do not go through the lower closure point any more.

For the desorption scanning curves we have attempted to use a simple scaling law similar to the one used for adsorption (see Eq. (2)), but we have faced the same problem that Mason had with his theoretical isotherms.

On the contrary, the approach proposed by Štěpánek and coworkers is based on recognizing that within the hysteresis loop the slope of the scanning curves at the turning points is of key importance. In particular the ratio between the slope of the adsorption curve reaching the turning point and that of the desorption curve leaving the turning point should reflect the qualitative trend observed in the experiments that Mason wanted to reproduce. They then decided to scale this ratio across the hysteresis loop in a predetermined manner and to use a reasonable functional form of the desorption isotherm (depending on two unknown parameters) to describe the whole desorption scanning curve (see Eq. (6)). The two parameters are chosen so as to make the desorption isotherm go through the turning point with the right slope (see Eq. (8)). Neither the pore connectivity nor the adjustable parameter introduced by Mason is needed any more.

It is rather clear that this approach is essentially empirical, and useful as far as it allows to describe scanning curves reasonably well. It is however also clear that there is some physical sense in defining the scanning curves through their slopes, insofar the slope of the scanning curves should reflect the emptying (and filling) of the pores at the given external conditions of relative humidity. This is the approach of choice in this work.

## 3 Implementation of the theory

The approach described in the previous section is applied to three adsorption isotherm models that are quite characteristic of water vapor adsorption on different adsorbents. The first is the same isotherm considered earlier (Štěpánek et al. 2000), i.e. the Dubinin–Radushkevich isotherm for adsorption and the Dubinin–Astakhov isotherm for desorption (DRA in short). The second is based on the Guggenheim–Anderson–de Boer model (GAB in short), and the third on the model proposed by Do and Do (2000) (DoDo in short). The parameters used in the numerical examples for the three isotherms are reported in Table 1.

### 3.1 Dubinin–Radushkevich and Dubinin–Astakhov model

The first example considers the isotherms used by Rajniak and Yang (1993, 1994) and later also by Štěpánek et al. (2000). For the primary adsorption isotherm the dual Dubinin–Radushkevich isotherm given by:

$$n_{\mathrm{A}}(x) = n_{\mathrm{s_1}}^{\infty} \exp\left[-\left(K_{\mathrm{s_1}} \ln\frac{1}{x}\right)^2\right] + n_{\mathrm{s_2}}^{\infty} \exp\left[-\left(K_{\mathrm{s_2}} \ln\frac{1}{x}\right)^2\right] \tag{9}$$

is used, while primary desorption is described by the Dubinin–Astakhov equation:

$$n_D(x) = n_L + n_{\mathrm{D}}^{\infty} \exp\left[-\left(K_D \ln\frac{1}{x - x_L}\right)^w\right] \tag{10}$$

Accordingly, the general desorption isotherm starting from point ($x_{2\mathrm{k}}$, $n_{2\mathrm{k}}$) is given by:

$$n_d(x) = n_{2\mathrm{k}-1} + n_{2\mathrm{k}}^{\infty} \exp\left[-\left(K_{2\mathrm{k}} \ln\frac{1}{x - x_{2\mathrm{k}-1}}\right)^w\right] \tag{11}$$

where the two parameters $n_{2\mathrm{k}}^{\infty}$ and $K_{2\mathrm{k}}$ have to be determined. Substituting Eqs. (9)–(11) into Eqs. (6) and (8) yields the following expressions for the parameters $K_{2\mathrm{k}}$ and $n_{2\mathrm{k}}^{\infty}$:

**Table 1** Numerical values for the DRA, GAB and DoDo models and the values for closure points of the corresponding hysteresis loops. The values for the DRA model were taken directly from Štěpánek et al. (2000)

| | Saturation capacity | | Parameters | | Closure points | | | |
|---|---|---|---|---|---|---|---|---|
| | | (mol kg$^{-1}$) | | (−) | | (−) | | (mol kg$^{-1}$) |
| DRA | $n_{\mathrm{s_1}}^{\infty}$ | 15.47 | $K_{\mathrm{s_1}}$ | 0.86 | | | | |
| | $n_{\mathrm{s_2}}^{\infty}$ | 3.77 | $K_{\mathrm{s_2}}$ | 0.12 | | | | |
| | $n_{\mathrm{D}}^{\infty}$ | 9.46 | $K_{\mathrm{D}}$ | 0.19 | $x_{\mathrm{L}}$ | 0.312 | $n_{\mathrm{L}}$ | 9.37 |
| | | | $w$ | 1.23 | $x_{\mathrm{U}}$ | 0.692 | $n_{\mathrm{U}}$ | 17.75 |
| GAB | $n^{\infty}$ | 0.958 | $k_{\mathrm{A}}$ | 1.01 | | | | |
| | | | $c_{\mathrm{A}}$ | 26.29 | | | | |
| | $n_{\mathrm{D}}^{\infty}$ | 1.00 | $k_{\mathrm{D}}$ | 1.26 | $x_{\mathrm{L}}$ | 0.302 | $n_{\mathrm{L}}$ | 1.27 |
| | | | $c_{\mathrm{D}}$ | 36.97 | $x_{\mathrm{U}}$ | 0.700 | $n_{\mathrm{U}}$ | 3.22 |
| DoDo | $n_{\mathrm{s}}^{\infty}$ | 0.0295 | $K_f$ | 4.39 | | | | |
| | $n_{\mu}^{\infty}$ | 4.39 | $K_{\mu}$ | 98.21 | | | | |
| | | | $m$ | 8.85 | | | | |
| | $n_{\mu,\mathrm{D}}^{\infty}$ | 3.7 | $K_{\mu,\mathrm{D}}$ | 80.00 | $x_{\mathrm{L}}$ | 0.500 | $n_{\mathrm{L}}$ | 0.83 |
| | | | $m_D$ | 1.27 | $x_{\mathrm{U}}$ | 0.831 | $n_{\mathrm{U}}$ | 4.35 |

$$K_{2k} = \left( \frac{\sigma_{2k} \Delta x}{w(w-1)\Delta n \ln\left[(\Delta x)^{-1}\right]} \right)^{1/w}$$
$$n_{2k}^{\infty} = \frac{\Delta n}{\exp\left(-\left(K_{2k} \ln\left[(\Delta x)^{-1}\right]\right)^{w}\right)} \quad (12)$$

Here the differences in relative humidity and adsorbed amount between the turning points 2k and (2k − 1) are defined as $\Delta x$ and $\Delta n$, respectively:

$$\Delta x = x_{2k} - x_{2k-1} \qquad \Delta n = n_{2k} - n_{2k-1} \quad (13)$$

These equations are the same as used earlier (Štěpánek et al. 2000), and are reposted here for the sake of clarity.

### 3.2 Guggenheim–Anderson–de Boer model

The GAB isotherm (Anderson 1946) is a modification of the Brunauer, Emmett, Teller (BET) isotherm. The BET model assumes two types of layers, namely the first and all the others, which are distinguished by two different values of the heat of adsorption, the one for the layers above the first being equal to the heat of condensation. The BET model has two parameters and the adsorbed amount approaches infinity when $x$ approaches one. The GAB model assumes three types of layers, the first layer, those between layer two and nine, and all the others. There are then three values of the heat of adsorption, thus yielding a three parameter model given by:

$$n_A(x) = \frac{n^{\infty} k_A c_A x}{(1 - k_A x)(1 + (c_A - 1)k_A x)} \quad (14)$$

The corresponding primary desorption branch is defined as:

$$n_D(x) = n_L + \frac{n_D^{\infty} k_D c_D (x - x_L)}{[1 - k_D(x - x_L)][1 + (c_D - 1)k_D(x - x_L)]} \quad (15)$$

The general desorption isotherm starting from the point ($x_{2k}$, $n_{2k}$) is given by:

$$n_d(x) = n_{2k-1} + \frac{n_D^{\infty} k_{2k} c_{2k} (x - x_{2k-1})}{[1 - k_{2k}(x - x_{2k-1})][1 + (c_{2k} - 1)k_{2k}(x - x_{2k-1})]} \quad (16)$$

where the two parameters $c_{2k}$ and $k_{2k}$ have to be determined using Eqs. (6) and (8). Their analytical expressions can be obtained easily:

$$c_{2k} = \frac{4 n_D^{\infty} (\Delta n)^3}{(n_D^{\infty} \sigma_{2k} \Delta x)^2 - (\Delta n)^2 (\Delta n - n_D^{\infty})^2}$$
$$k_{2k} = \frac{(\Delta n)^2 - n_D^{\infty} \Delta n + n_D^{\infty} \sigma_{2k} \Delta x}{\Delta x \left( (\Delta n)^2 + n_D^{\infty} \Delta n + n_D^{\infty} \sigma_{2k} \Delta x \right)} \quad (17)$$

### 3.3 Do and Do model

The DoDo model assumes two contributions to the amount of water adsorbed on activated carbon (AC), $n_A(x)$. At low relative humidity functional groups on the surface of AC, that represent high energy sites, are occupied by water molecules, and successive clustering of the water molecules around these sites is represented by $n_s(x)$. The adsorption in the pores at medium to high relative humidity is represented by the term $n_\mu(x)$ (Do and Do 2000). Therefore, the adsorbed amount of water is given by:

$$n_A(x) = n_s(x) + n_\mu(x)$$
$$n_A(x) = \frac{n_s^{\infty} K_f x}{(1 - x)(1 + (K_f - 1)x)} + \frac{n_\mu^{\infty} K_\mu x^m}{1 + K_\mu x^m} \quad (18)$$

which represents the primary adsorption isotherm. The inherent assumption of the percolation model of hysteresis that is used by Štěpánek et al. (2000) is that adsorption as well as desorption occurs in the pore space of the adsorbent. Accordingly, in order to calculate the desorption branch only $n_\mu(x)$ is considered here, and the primary desorption branch is thus given by:

$$n_D(x) = n_L + \frac{n_{\mu,D}^{\infty} K_{\mu,D} (x - x_L)^{m_D}}{1 + K_{\mu,D}(x - x_L)^{m_D}} \quad (19)$$

The general desorption isotherm starting from point ($x_{2k}$, $n_{2k}$) is therefore given by:

$$n_d(x) = n_{2k-1} + \frac{n_{2k}^{\infty} K_{2k} (x - x_{2k-1})^{m_D}}{1 + K_{2k}(x - x_{2k-1})^{m_D}} \quad (20)$$

where $n_{2k}^{\infty}$ and $K_{2k}$ are determined through Eqs. (6) and (8) and are calculated as follows:

$$n_{2k}^{\infty} = \frac{m_D \Delta n^2}{m_D \Delta n - \sigma_{2k} \Delta x}$$
$$K_{2k} = \frac{m_D \Delta n^2}{n_{2k} \sigma_{2k} (\Delta x)^{m_D + 1}} \quad (21)$$

### 3.4 Scanning curves and embedded adsorption/desorption loops

An overview of the primary adsorption and desorption branches of the three isotherm models discussed above is given in Fig. 1. According to the IUPAC classification of adsorption types, the Dubinin–Radushkevich model is of type IV, while the GAB and DoDo models are of type II and V, respectively. The hysteresis types according to the IUPAC classification are type H2 for both the DRA and DoDo models, while the GAB hysteresis loop cannot be uniquely classified. The GAB model was chosen for this work for its relation to experimental data of water

adsorption and desorption on zeolite ZSM-5 measured in our lab. In addition, the DoDo model was chosen based on experimental data of water adsorption and desorption on activated carbon.

Figure 2 zooms into the region of the hysteresis loops of the three isotherm models. Figure 2a shows four secondary desorption scanning curves for the DRA model as calculated with the methodology described above. The model used here describes scanning curves of the 'converging type' (Tompsett et al. 2005), i.e. all four scanning curves end in the lower closure point, which is their lower validity limit. This is true for all scanning curves that emerge from the primary adsorption branch. The same features are observed in Fig. 2c and e, which contain four scanning curves for the GAB isotherm and the DoDo isotherm model, respectively. These characteristics are typical of the description of scanning curves based on a pore network model (Tompsett et al. 2005).

Figure 2b shows two embedded hysteresis loops for the DRA model, while Fig. 2d and f show two embedded hysteresis loops for the GAB and DoDo isotherm models, respectively. The arrows indicate if the curve is a desorption scanning curve (arrowhead down), or an adsorption scanning curve (arrowhead up). Note that it is possible that the scanning curves cross. The direction of the path after the crossing point depends on the history, thus illustrating the memory dependence of hysteresis curves (Rajniak and Yang 1994).

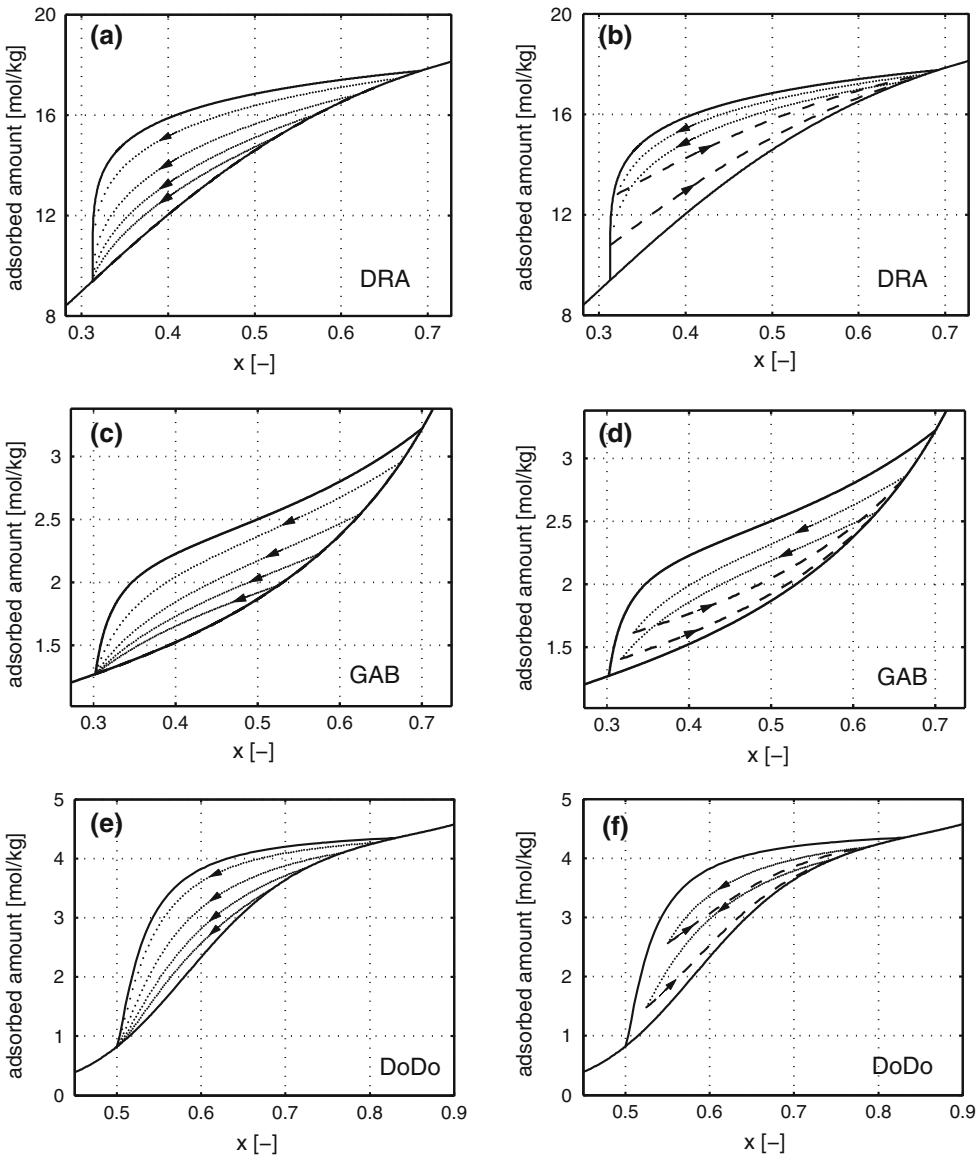


**Fig. 2** Scanning curves for the DRA, GAB and DoDo models. Subfigures **a**, **c** and **e** show secondary desorption scanning curves at equidistant intervals for the DRA, the GAB and the DoDo isotherm model, respectively, while subfigures **b**, **d** and **f** show two embedded hysteresis loops that started at two different points. For the sake of clarity only the relevant range of relative humidity $x$ was plotted

## 4 Modeling water vapor adsorption/desorption cycles

In this section we present the assumptions made to model the behavior of a fixed adsorption bed under non-isothermal conditions and report the model equations. Then, we describe the solution algorithm developed to account for the memory effects that are of crucial importance in the cases where the adsorbate exhibits hysteresis. Finally, for each of the three adsorption isotherms introduced in Sect. 3, we present and discuss three different adsorption/desorption cycles as case studies.

### 4.1 Model equations

The mathematical model of adsorption/desorption in a fixed adsorption bed is based on the following assumptions:

- One-dimensional column with negligible radial concentration and temperature gradients;
- Mass transfer described by the linear driving force model, where the mass transfer coefficient is a lumped parameter and is independent of temperature and loading;
- Isosteric heat of adsorption loading independent and equal to the heat of condensation in the case of water vapor;
- Heat capacities of the solids temperature independent;
- Pressure drop negligible along the column.

With these assumptions the resulting partial differential equations (PDEs) are summarized in Table 2; a more detailed description of the column model is reported by Casas et al. (2012) and is not repeated here for the sake of brevity.

The finite volume method is used to discretize in space the system of PDEs in Table 2. Flux limiters following Van Leer's method were used to stabilize the time integration, which was performed with a commercial IMSL DIVPAG solver (Fortran) using Gear's method (Casas et al., 2012). The numerical parameters used for the simulations are given in Table 3.

**Table 2** Summary of the system of partial differential equations that describes the adsorption column

Component and mass balances:

$$\varepsilon_t \frac{\partial c}{\partial t} + \frac{\partial (uc)}{\partial z} + \rho_b \sum_{i=1}^{N} \frac{\partial n_i}{\partial t} = 0$$

$$\varepsilon_t \frac{\partial c_i}{\partial t} + \frac{\partial (uc_i)}{\partial z} + \rho_b \frac{\partial n_i}{\partial t} - \varepsilon_b \frac{\partial}{\partial z}\left(D_L c \frac{\partial y_i}{\partial z}\right) \quad i = 1, \ldots, N$$

Linear driving force model:

$$\frac{\partial n_i}{\partial t} = k_i (n_i^* - n_i) \quad i = 1, \ldots, N$$

Energy balance for the solid and fluid phase:

$$\left(\varepsilon_t C_g + \rho_b C_s + \rho_b C_{ads}\right) \frac{\partial T}{\partial t} - \varepsilon_t \frac{\partial p}{\partial t}$$

$$+ u C_g \frac{\partial T}{\partial z} - \rho_b \sum_{i=1}^{N} (-\Delta H_i) \frac{\partial n_i}{\partial t}$$

$$+ \frac{2h_L}{R_i}(T - T_w) - \varepsilon_b \frac{\partial}{\partial z}\left(K_L \frac{\partial T}{\partial z}\right) = 0$$

Energy balance for the column wall:

$$\frac{\partial T_w}{\partial t} = \frac{2}{C_w\left(R_0^2 - R_i^2\right)}\left(h_L R_i (T - T_w) - h_w R_0 (T_w - T_{amb})\right)$$

Equation of state:

$$c_i = \frac{y_i P}{RT}$$

$c$ is the total fluid phase concentration, $c_i$ and $n_i$ are the fluid and adsorbed concentration of species $i$; $\varepsilon_t$, $\varepsilon_b$, $u$ and $\rho_b$ are the overall and bed void fraction, the superficial gas velocity and the bulk density of the packing in the column, respectively. $D_L$ is the axial despersion coefficient and $y_i$ is the mole fraction of component $i$ in the gas phase. $k_i$ is the lumped mass transfer coefficient of component $i$ and $n_i^*$ is the adsorbed amount at equilibrium. For the energy balances $C_g$, $C_s$ and $C_{ads}$ (calculated during the simulation) are the heat capacities of the fluid, the solid and the adsorbed phase, respectively; $\Delta H_i$ is the isosteric heat of adsorption of component $i$; $h_L$ is the heat transfer coefficient from inside the column to the column wall; $R_i$ and $R_0$ are the inner and outer radii of the column and $K_L$ is the axial thermal conductivity; $h_w$ and $C_w$ are the heat transfer coefficient from the wall to the environment and the heat capacity of the column wall, respectively. Finally, $T$, $p$ and $R$ are the temperature, pressure and the universal gas constant, respectively

### 4.2 Implementation of hysteresis dependent isotherms

The model equations in Table 2 are general, i.e. they apply to both cases, i.e. with or without hysteresis. However, the algorithm solving the equations is rather different when the adsorption isotherm exhibits hysteresis.

A flowchart of the algorithm used to account for hysteresis dependent isotherms is given in Fig. 3. The first main difference to a conventional case without hysteresis is that the process history has to be stored. In particular, this requires a memory or stack that is accessible at every point in time during the simulation. This memory has dimensions $N_g \times N_t \times N_p$, where $N_g$ corresponds to the number of gridpoints used for the discretization in space, $N_t$ the number of previous turning points and $N_p$ the number of parameters that are stored. The second main difference is that depending on being in the adsorption or in the desorption mode different isotherms must be used to describe the equilibrium amount adsorbed.

If the initial conditions are such that the column is saturated at a humidity that lies within the hysteresis loop, i.e. between $x_L$ and $x_U$, it has to be specified if this state was attained by wetting or drying. In the former case, the starting point of the equilibrium isotherm is the primary adsorption branch, while in the latter case, the correct starting value is on the primary desorption branch. If the humidity of the feed is below the initial humidity (desorbing conditions) and the initial state was attained by wetting, the equilibrium relationship will be given by a secondary desorption scanning curve, the parameters of which are calculated according to Eqs. (6) and (8). On the other hand, if the humidity of the feed is higher than the

**Table 3** Parameters for the adsorption column model

| Parameter | | Value | |
|---|---|---|---|
| Column length | $L$ | 0.2 | m |
| Inner column radius | $R_i$ | 0.025 | m |
| Outer column radius | $R_0$ | 0.050 | m |
| Bulk density of the packing | $\rho_b$ | 507 | kg $m^{-3}$ |
| Particle density | $\rho_p$ | 850 | kg $m^{-3}$ |
| Bed porosity | $\epsilon_b$ | 0.4 | (−) |
| Particle size | $d_p$ | $0.3 \times 10^{-3}$ | m |
| Mass transfer coefficient for $H_2O$ | $k_i$ | $6.43 \times 10^{-3}$ | $s^{-1}$ |
| Dispersion coefficient | $D_L$ | $6.5 \times 10^{-5}$ | $m^2$ $s^{-1}$ |
| Solid heat capacity | $C_s$ | 1250 | J $K^{-1}$ $kg^{-1}$ |
| Gas heat capacity | $C_g$ | 42.46 | J $K^{-1}$ $mol^{-1}$ |
| Heat transfer coefficient (fluid-wall) | $h_L$ | Variable | J $K^{-1}$ $mol^{-1}$ |
| Heat transfer coefficient (lumping wall + heating) | $h_w$ | 5 | J $K^{-2}$ $mol^{-1}$ |
| Axial thermal conductivity in the fluid phase | $K_L$ | 0.04 | J $m^{-1}$ $s^{-2}$ $K^{-1}$ |
| Isotherm parameters | See Table 1 | | |
| Heat of adsorption $H_2O$ | $\Delta H_{H_2O}$ | −40 | kJ $mol^{-1}$ |

The value for the mass transfer coefficient was taken from Štěpánek et al. (2000)

initial humidity (adsorbing conditions) and the initial state was attained by drying, the equilibrium relationship will be given by a secondary adsorption scanning curve according to Eq. (2). This procedure is schematically illustrated by the Algorithm 1 shown in Fig. 4a.

Whenever a mode transition (that is a switch from adsorption condtitions to desorption conditions or vice versa) occurs during the process, a turning point is calculated and, provided that it is within the hysteresis loop, the turning point is used to calculate new isotherm parameters (Štěpánek et al. 2000). On the other hand, if the turning point does not lie within the range of hysteresis the stack is reset to its initial state. This simple procedure is schematically illustrated by the Algorithm 2 shown in Fig. 4b.

A crucial feature of the implementation is to consider the validity limits of the scanning curves. Therefore, it is useful to consider the primary adsorption and desorption branches first. If the system is under desorbing conditions and the relative humidity drops below the relative humidity of the lower closure point, $x_L$, the adsorption and desorption branch overlap. Accordingly, if the system is under adsorbing conditions and the relative humidity exceeds the relative humidity of the upper closure point, $x_U$, the adsorption and desorption branch also coincide. The same logic applies to the scanning curves. The lower closure point or validity limit of a general desorption scanning curve starting from the turning point $(x_{2k}, n_{2k})$, is the previous turning point $(x_{2k-1}, n_{2k-1})$.

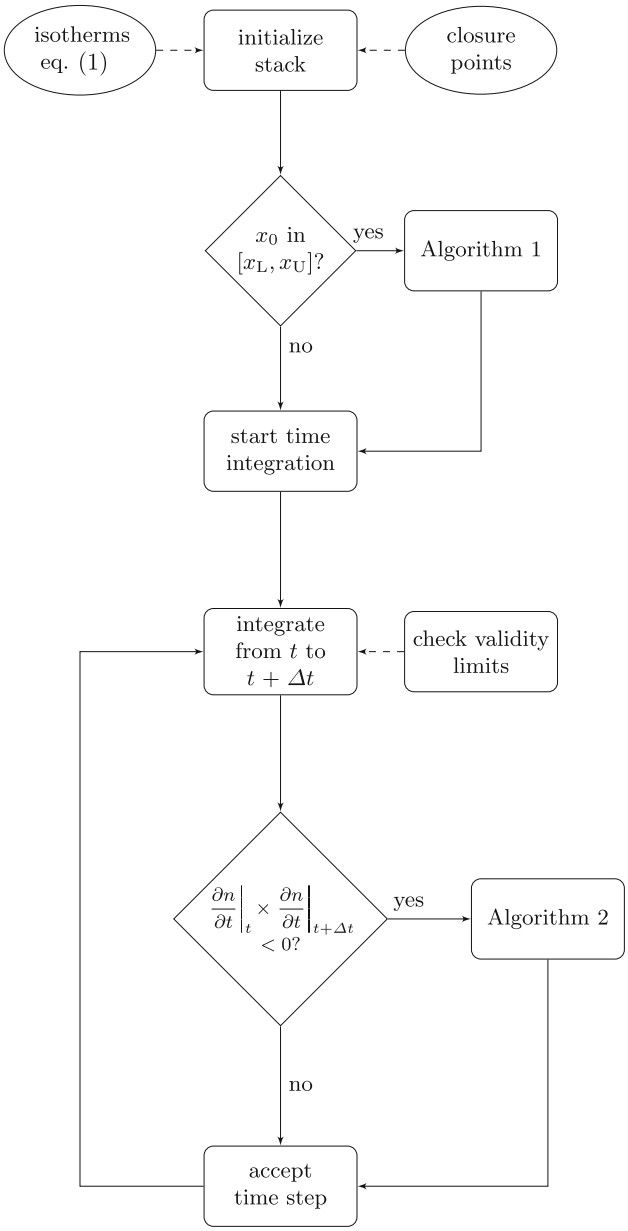


**Fig. 3** Schematic representation of implementation of hysteresis dependent isotherms. As illustrated, the inputs for the algorithm are the isotherm equations as well as the closure points. Refer to Fig. 4 for Algorithms 1 and 2

If the relative humidity drops below $x_{2k-1}$, the scanning curve will follow the most recent desorption scanning curve. In the algorithm, this requires the release of the current desorption scanning curve parameters and the use of the most recent ones. In case of an adsorption scanning curve starting from the turning point $(x_{2k-1}, n_{2k-1})$, the previous turning point $(x_{2k-2}, n_{2k-2})$ has similar characteristics as the upper closure point of the primary hysteresis loop. If the relative humidity exceeds $x_{2k-2}$ the adsorption scanning curve will follow the most recent adsorption scanning curve. Accordingly, the

```
Algorithm 1
if mode=adsorption then
  if n_0 ∈ n_A(x) then
    go to 'start time integration'
  else
    update stack
    calculate new parameters
  end if
else
  if mode=adsorption then
    update stack
    calculate new parameters
  else
    go to 'start time integration'
  end if
end if
```

**(a)** Algorithm 1 is used to determine if the initial conditions are such that the equilibrium is described by a scanning curve. $n_0$ is the initial loading.

```
Algorithm 2
calculate turning point
if x_L ≤ x_tp ≤ x_U then
  update stack
  calculate new parameters
else
  reset stack
end if
```

**(b)** Algorithm 2 is used to decide if the new parameters need to be calculated or the stack has to be reset. $x_{tp}$ is the relative humidity at the turning point.

**Fig. 4** Algorithms 1 and 2 used for the implementation of adsorption isotherms exhibiting hysteresis. Subfigures **a** and **b** are parts of Fig. 3

algorithm releases the current adsorption scanning curve parameters and the most recent parameters are recalled.

In this study, it is assumed that the temperature dependence of the isotherm models is accounted for by the temperature dependence of the vapor pressure. Thus, when plotted against relative humidity the sorption isotherms at different temperatures overlap. This is consistent with the assumption that the heat of adsorption equals the heat of condensation. In fact, such behavior in the case of water adsorption has been reported in the literature (Leppäjärvi et al. 2012, 2013). Moreover, it is assumed that the hysteresis loop is independent of temperature in the range considered in this study. Although this is not completely true in general (Horikawa et al. 2011), we have made preliminary measurements that are consistent with this assumption.

### 4.3 Simulation of adsorption/desorption cycles

In this section we report about the application of the model above, particularly to the three adsorption isotherms introduced in Sect. 3. For each isotherm, the same adsorption/desorption cycle has been simulated under three different conditions in terms of heat transfer, namely under isothermal conditions (heat transfer is infinitely fast to remove the heat of adsorption or to provide the heat of desorption), under adiabatic conditions (heat transfer is infinitely slow), and under conditions typical of a lab-scale fixed bed column, i.e. where heat transfer is neither infinitely fast nor infinitely slow but it is determined through a proper heat transfer equation and the corresponding heat transfer coefficient. In Figs. 5, 6 and 7 we show the adsorption and desorption water vapor profile from start of the simulation, to column saturation at the feed conditions, and then back to the initial conditions (black and blue lines). Together with it, we also show the temperature profile at the column outlet (red lines), with the exception of the case where the simulation is isothermal. The simulated operating conditions are summarized in Table 4. Note that the time scale has been adjusted in every plot in order to offer the best visualization of the concentration fronts; as a consequence the comparison of the dynamics exhibited by the different simulations should be made by carefully considering the prevailing scale of the time axis.

#### *4.3.1 Role of hysteresis*

All simulations have also been performed by pretending that the adsorbate does not exhibit hysteresis. In all plots the profiles obtained through simulations accounting for hysteresis are plotted as dashed lines, while the solid lines represent simulations without hysteresis. The two simulations are indistinguishable during adsorption (since in all cases adsorption starts outside of the hysteresis loop and follows the primary adsorption isotherm), but differ during desorption as expected. The differences are larger, the larger the hysteresis loop (see Fig. 1). While in the GAB case the two profiles are very similar, and the differences are possibly smaller than the uncertainty in the adsorption isotherm itself, in the DRA case the differences cannot be ignored, the case of the DoDo isotherm being somewhat in between the other two.

#### *4.3.2 Role of heat effects*

In the case of all three isotherms the three simulations under isothermal, adiabatic and intermediate conditions yield rather different results. This does not have necessarily to do with the presence of the hysteresis loop, but with the fact that water vapor exhibits significant heat of adsorption that causes major heat effects. As the rate of heat transfer is reduced from the figure at the top (isothermal) to that at the bottom (adiabatic), the time needed to saturate the column (at the feed concentration and temperature) and the time to regenerate it become increasingly long; this is understandable as the heat of adsorption and the heat of desorption have to be removed and provided, respectively, through the gas flow itself.

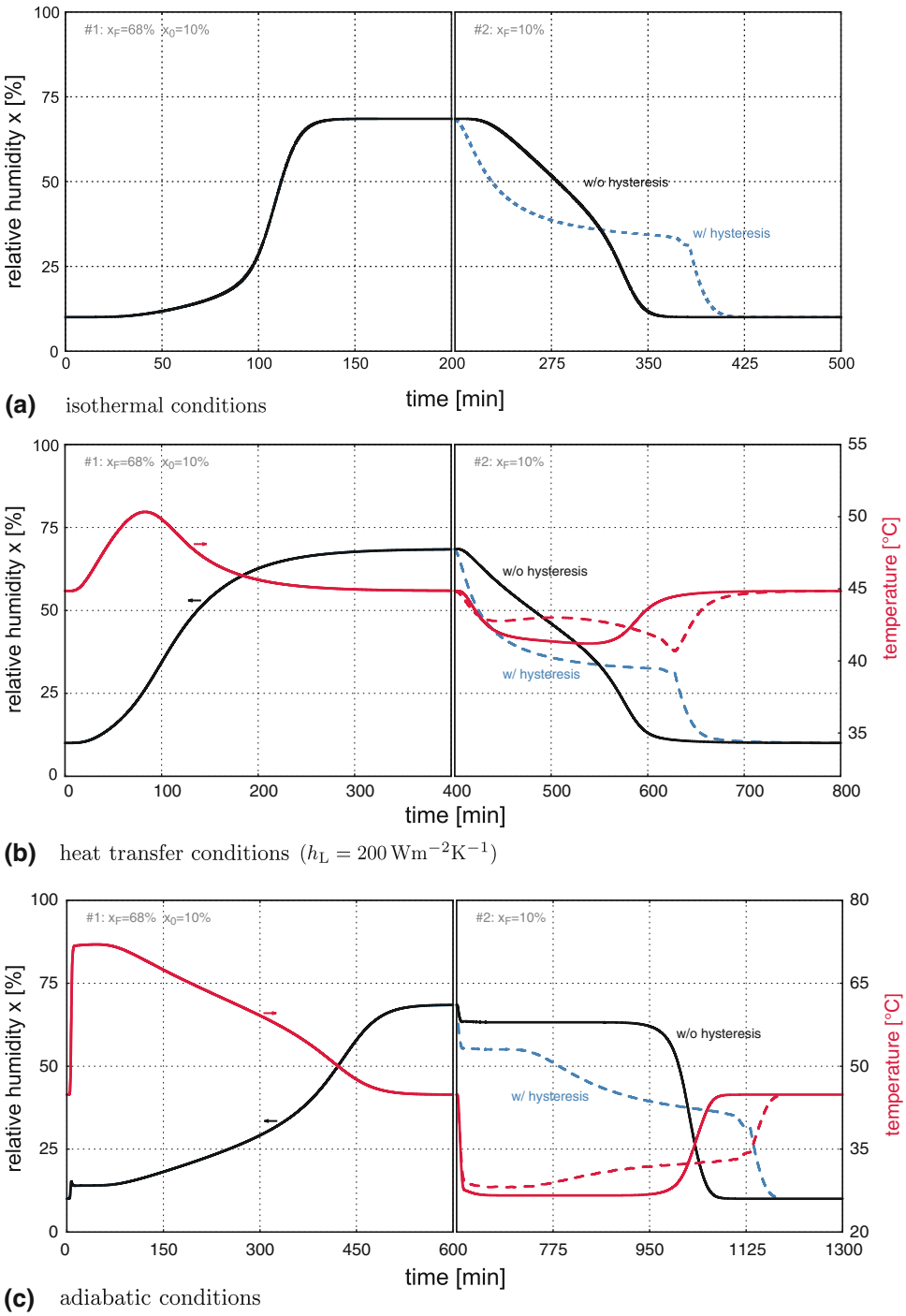


**Fig. 5** Breakthrough simulations at three sets of conditions for the DRA model. As labelled in the subfigures, the *solid lines* are the simulation results considering the DRA model without hysteresis, whereas the *dashed lines* indicate the results with taking hysteresis into account. The *red curves* represent the temperature profiles and are plotted against the *right y-axis*. The values of the parameters used for the simulations as well as the initial and feed conditions are summarized in Tables 3 and 4, respectively (Color figure online)

#### *4.3.3 Role of isotherm*

Since the three adsorption isotherms considered here have rather different shapes, as a consequence the calculated adsorption and desorption profiles are rather different. This is not surprising, but it is nevertheless interesting and useful to see.

## 5 Discussion and conclusions

This work is based on the method developed by Štěpánek and coworkers to describe adsorption and desorption scanning curves for a species that exhibits capillary condensation and a hysteresis loop. The interest for this system stems from the fact that water vapor is one such species and

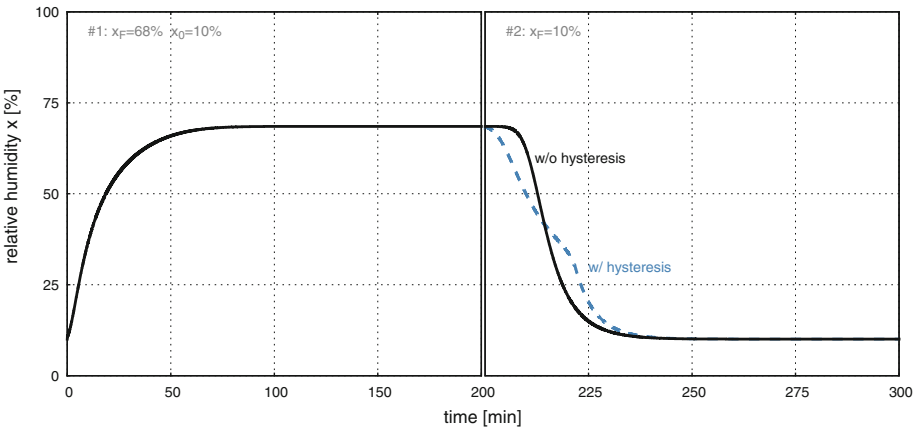


**(a)** isothermal conditions

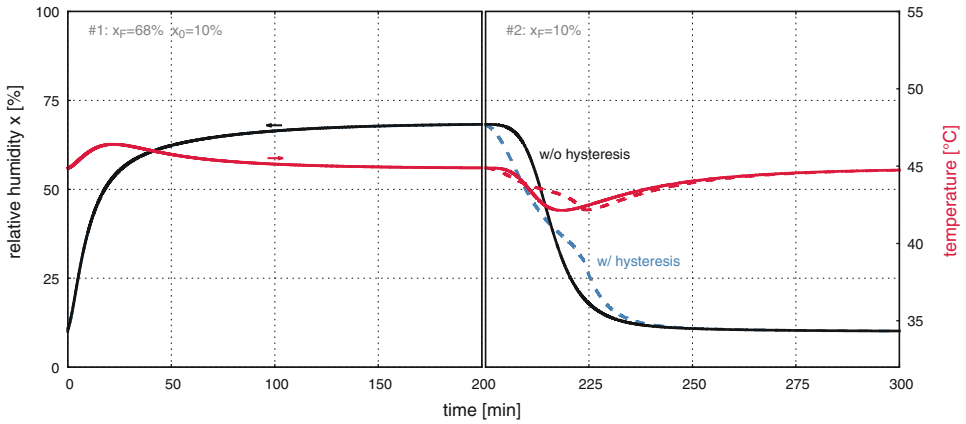


**(b)** heat transfer conditions ($h_{\mathrm{L}} = 200\,\mathrm{Wm^{-2}K^{-1}}$)

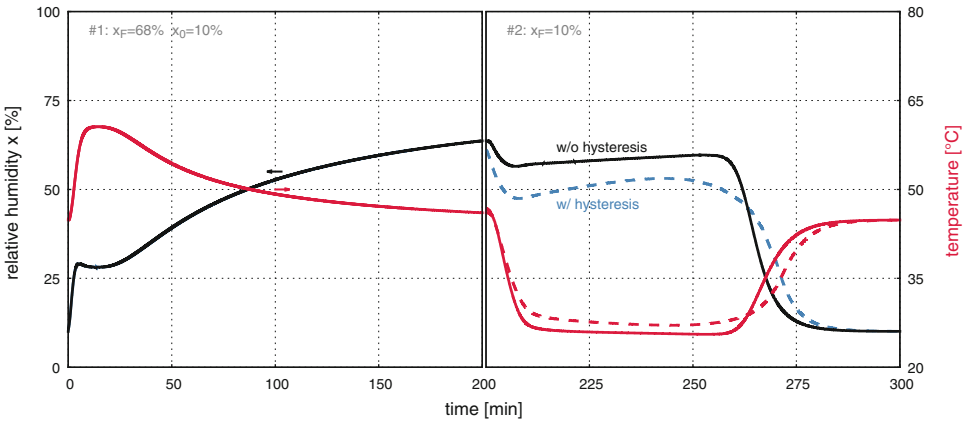


**(c)** adiabatic conditions

**Fig. 6** Breakthrough simulations at three sets of conditions for the GAB model. As labelled in the subfigures, the *solid lines* are the simulation results considering the GAB model without hysteresis, whereas the *dashed lines* indicate the results with taking hysteresis into account. The *red curves* represent the temperature profiles and are plotted against the *right y-axis*. The values of the parameters used for the simulations as well as the initial and feed conditions are summarized in Tables 3 and 4, respectively (Color figure online)

it plays a key role in many important applications of adsorption.

We have expanded that method in two ways, thus bringing a few novel elements to the discussion about how to include water vapor into the simulation of adsorption processes of interest, such as the capture of carbon dioxide in near-zero-emission power plants. Firstly, based on a few reasonable assumptions, we have derived the adsorption/desorption scanning curves for two more isotherms, GAB and DoDo, which have proven to be useful in describing water vapor adsorption on different materials. Secondly, we have applied the approach to modeling adsorption/

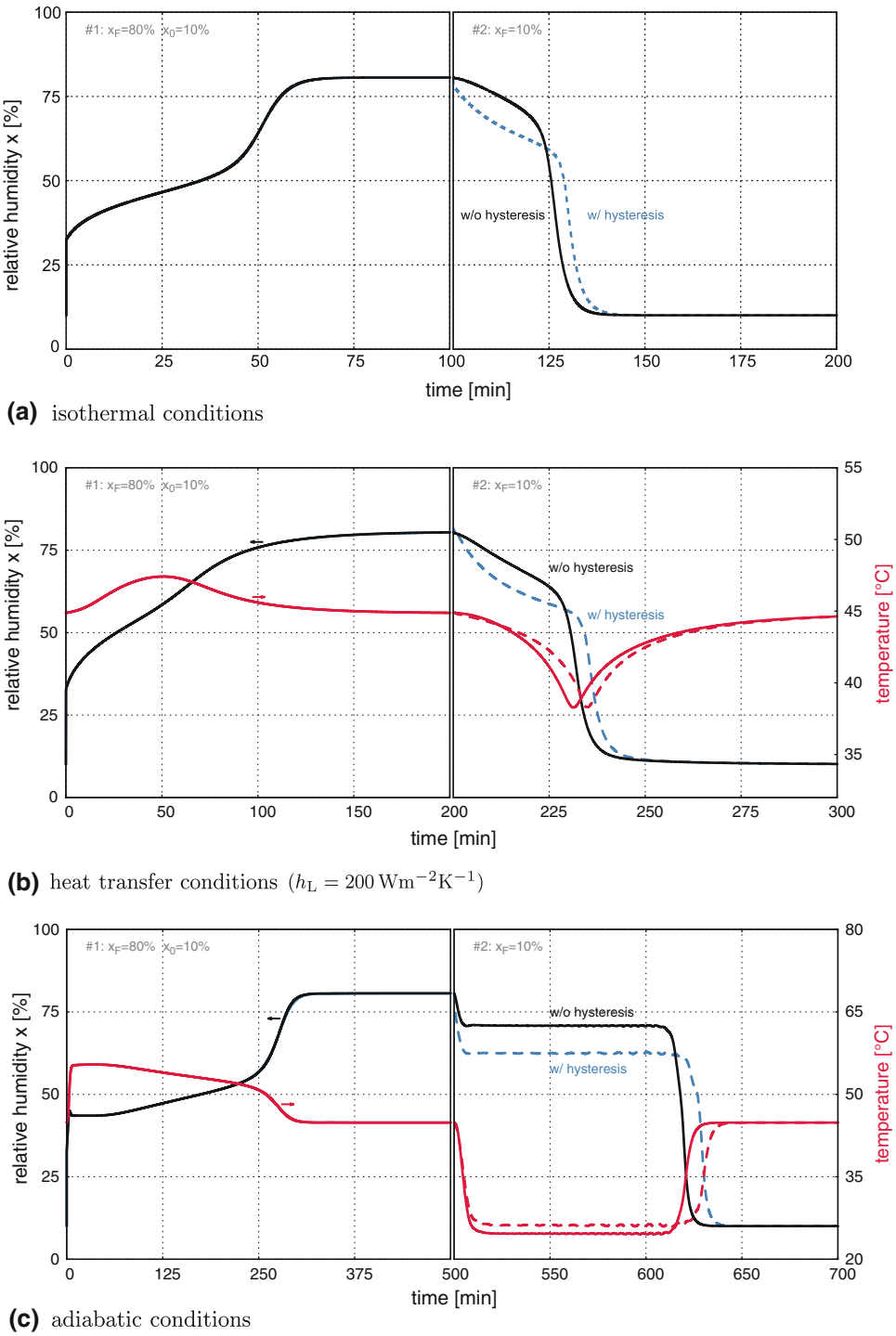


**Fig. 7** Breakthrough simulations at three sets of conditions for the DoDo model. As labelled in the subfigures, the *solid lines* are the simulation results considering the DoDo model without hysteresis, whereas the *dashed lines* indicate the results with taking hysteresis into account. The *red curves* represent the temperature profiles and are plotted against the *right y-axis*. The values of the parameters used for the simulations as well as the initial and feed conditions are summarized in Tables 3 and 4, respectively (Color figure online)

desorption cycles in a fixed bed to more general situations than the isothermal case considered in the original publication (Štěpánek et al. 2000). Both elements of novelty expand the applicability of the existing method significantly.

While on the one hand we have shown that the model can be applied effectively to rather general cases, it is on the other hand clear that the accuracy of the fixed bed simulations and their predictive capability is limited by the accuracy of the rather empirical approach adopted by Štěpánek and coworkers and by us in this work to obtain the adsorption/desorption scanning curves. Unfortunately, the scarcity of water vapor adsorption data and of experimental evidence on the shape and location of the scanning curves makes it difficult to assess the accuracy of the model. We believe that it is important to make an effort to obtain more accurate and reliable experimental data both about adsorption isotherms

**Table 4** Initial and feed conditions used for adsorption/desorption cycle simulations

| Initial conditions | | | |
|---|---|---|---|
| Temperature | $T$ | 45 | °C |
| Pressure | $p_0$ | 1 | bar |
| Relative humidity for (DRA, GAB, DoDo) | $x_0$ | 10 | % |
| **Feed conditions** | | | |
| Velocity | $u$ | 0.1 | m $s^{-1}$ |
| Temperature | $T$ | 45 | °C |
| Pressure | $p_F$ | 1 | bar |
| Relative humidity for DRA,GAB | $x_F$ | 68 | % |
| Relative humidity for DoDo | $x_F$ | 80 | % |

of water (through static experiments for example in a gravimetric set-up) and about fixed bed adsorption/desorption cycles (through dynamic experiments in a fixed bed). Once more water vapor adsorption data are available it will be possible to refine the model description of this important and fascinating phenomenon.

**Acknowledgments** Support of the Swiss National Science Foundation through grant NF 200021-130186 is gratefully acknowledged.

## References

Anderson, B.: Modifications of the Brunauer, Emmett and Teller equation. J. Am. Chem. Soc. **68**(7), 686–691 (1946)

Casas, N., Schell, J., Pini, R., Mazzotti, M.: Fixed bed adsorption of CO2/H2 mixtures on activated carbon: experiments and modeling. Adsorption **18**(2), 143–161 (2012)

Do, D.D., Do, H.D.: A model for water adsorption in activated carbon. Carbon **38**, 767–773 (2000)

Horikawa, T., Do, D.D., Nicholson, D.: Capillary condensation of adsorbates in porous materials. Adv. Colloid Interface Sci. **169**(1), 40–58 (2011)

Leppäjärvi, T., Malinen, I., Kangas, J., Tanskanen, J.: Utilization of Pisat temperature-dependency in modelling adsorption on zeolites. Chem. Eng. Sci. **69**, 503–513 (2012)

Leppäjärvi, T., Kangas, J., Malinen, I., Tanskanen, J.: Mixture adsorption on zeolites applying the temperature-dependency approach. Chem. Eng. Sci. **89**, 89–101 (2013)

Mason, G.: A model of adsorption–desorption hysteresis in which hysteresis is primarily developed by the interconnections in a network of pores. Proc. R. Soc. A **390**(1798), 47–72 (1983)

Mason, G.: Determination of the pore-size distributions and of Vycor porous glass from adsorption-desorption hysteresis capillary condensation isotherms. Proc. R. Soc. A **415**(1849), 453–486 (1988)

Mualem, Y.: Modified approach to capillary hysteresis based on a similarity hypothesis. Water Resour. Res. **9**(5), 1324–1331 (1973)

Mualem, Y., Beriozkin, a.: General scaling rules of the hysteretic water retention function based on Mualems domain theory. Eur. J. Soil Sci. **60**(4), 652–661 (2009)

Philip, J.R.: Similarity hypothesis for capillary hysteresis in porous materials. J. Geophys. Res. **69**(8), 1553–1562 (1964)

Rajniak, P., Yang, R.T.: A simple model and experiments for adsorption-desorption hysteresis: water vapor on silica gel. AIChE J. **39**(5), 774–786 (1993)

Rajniak, P., Yang, R.T.: Hysteresis-dependent adsorption–desorption cycles: generalization for isothermal conditions. AIChE J. **40**(6), 913–924 (1994)

Rajniak, P., Yang, R.T.: Unified network model for diffusion of condensable vapors in porous media. AIChE J. **42**(2), 319–331 (1996)

Tompsett, Ga., Krogh, L., Griffin, D.W., Conner, W.C.: Hysteresis and scanning behavior of mesoporous molecular sieves. Langmuir **21**(18), 8214–25 (2005)

Štěpánek, F., Kubíček, M., Marek, M., Šoóš, M., Rajniak, P., Yang, R.T.: On the modeling of PSA cycles with hysteresis-dependent isotherms. Chem. Eng. Sci. **55**(2), 431–440 (2000)